GEOPHYSICAL RESEARCH LETTERS, VOL. 35, L08605, doi:10.1029/2008GL033263, 2008

Megatides in the Arctic Ocean under glacial conditions

Stephen D. Griffiths,[1] and W. R. Peltier[1]

Received 11 January 2008; revised 11 March 2008; accepted 28 March 2008; published 29 April 2008.

[1] Over the history of the Earth, changes in ocean depth and coastal configuration have led to considerable variations in the pattern and amplitude of ocean tides. Here we perform global simulations of ocean tides for the Last Glacial Maximum, using new data sets for both ocean depth and density stratification. We show how the configuration of the Arctic Ocean, which was almost entirely enclosed by continents at that time, leads to the near-resonant excitation of large semi-diurnal tides. Under certain conditions, this previously unidentified Arctic tide is massively amplified in the Canadian Archipelago. Such tides may have played a role in destabilizing the coastal margins of North American ice sheets, with implications for rapid changes in the Earth's climate and ocean circulation.
Citation: Griffiths, S. D., and W. R. Peltier (2008), Megatides in the Arctic Ocean under glacial conditions, *Geophys. Res. Lett.*, *35*, L08605, doi:10.1029/2008GL033263.

1. Introduction

[2] Ocean tides are the response of a forced-dissipative oscillatory system. The solar and lunar forcing, which has a simple geometrical form, occurs at various frequencies, principally with diurnal or semi-diurnal timescales. However, the response is far from simple, being dominated by signals where, due to the bathymetry, free-waves are near resonant at the forcing frequency. The dissipation occurs via two frictional processes: drag from a turbulent bottom boundary layer (which is strong in shallow marginal seas), and drag from an internal tide which is generated because the ocean is density stratified (and which is strong over steep topography in the deep ocean [e.g., *Garrett and Kunze*, 2007]).

[3] Even relatively small topographic changes can shift free waves towards or away from resonance for a given tidal constituent. Thus, during the glacial periods of the Late Pleistocene, when large continental ice sheets existed in the northern hemisphere and sea level was lowered by approximately 120 m, the tides would have been different from those of the present-day ocean. Such glacial conditions are of special interest, because they have occurred quasi-periodically and accounted for the most extreme topographic changes over the Late Pleistocene. We will focus on tides at the Last Glacial Maximum (LGM), which occurred approximately 26,000 years ago, since the bathymetric changes are now well constrained [*Peltier and Fairbanks*, 2006] by the ICE-5G v 1.2 data set [*Peltier*, 2004]. As shown in Figure 1, at LGM there were significant changes in the coastal configurations of the Arctic, North Atlantic, and western Pacific Oceans. We shall show how this led to a significant amplification of tides in the Arctic Ocean.

[4] However, Arctic tides cannot be considered in isolation, and must be modeled as part of a global tidal solution. Note that the predicted eustatic sea level fall of about 120 m, now independently verified by *Biton et al.* [2008], implies that the shallow marginal seas of the present-day ocean had effectively disappeared at LGM. Drag in the shallow seas is the dominant source of tidal dissipation in the present-day, at least in a globally integrated sense [e.g., *Egbert and Ray*, 2003], but at LGM internal tide drag (in the deep ocean) must have played a major role in setting tidal amplitudes and dissipation [*Egbert et al.*, 2004; *Wunsch*, 2005]. Thus, a careful consideration of the ocean stratification at LGM is crucial to obtaining realistic tides, either on a global scale or in the Arctic Ocean.

[5] Although available data for LGM is sparse [e.g., *Adkins et al.*, 2002], ocean stratification can be estimated from the coupled atmosphere-ocean climate simulations of *Peltier and Solheim* [2004], which were performed for both present-day and LGM conditions. From the final 50 years of these simulations, we calculated the time-averaged vertically-averaged buoyancy frequency N, as shown in Figure 1. Much of the spatial variation simply correlates with ocean depth, with large values of N in the shallow marginal seas, and smaller values in the deep ocean. In waters deeper than 1000 m, the present-day modeled values for N have a global average of 2.9×10^{-3} s^{-1}, and a globally averaged error of 1.0×10^{-3} s^{-1} (measured against observed values according to the World Ocean Atlas 2005). At LGM, N is slightly reduced in general, with a global average of 2.6×10^{-3} s^{-1}. A notable exception is in the North Atlantic and Arctic Oceans, where a freshening of the surface waters and a salinification of the deep ocean causes N to increase. The implied enhanced internal tide drag in the North Atlantic might play a role in moderating tides there, a region which is key for the forcing of Arctic tides.

2. Numerical Modeling of Global Tides

[6] We have used these topographic and stratification data sets to model tides at LGM. Writing the depth-averaged horizontal flow as $\mathbf{u}$ and the free-surface displacement as ζ, we model tides as a shallow water flow:

$$\frac{\partial \mathbf{u}}{\partial t} + \mathbf{f} \times \mathbf{u} = -g\nabla(\zeta - \zeta_{EQ} - \zeta_{SAL}) - \frac{\mathbf{D}_{BL} + \mathbf{D}_{IT}}{\rho H},$$

$$\frac{\partial \zeta}{\partial t} + \nabla \cdot (H\mathbf{u}) = 0.$$

Here $\mathbf{f}$ is the vertical component of the Coriolis parameter, H is the undisturbed ocean depth, g is the acceleration due

[1]Department of Physics, University of Toronto, Toronto, Ontario, Canada.

0094-8276/08/2008GL033263$05.00

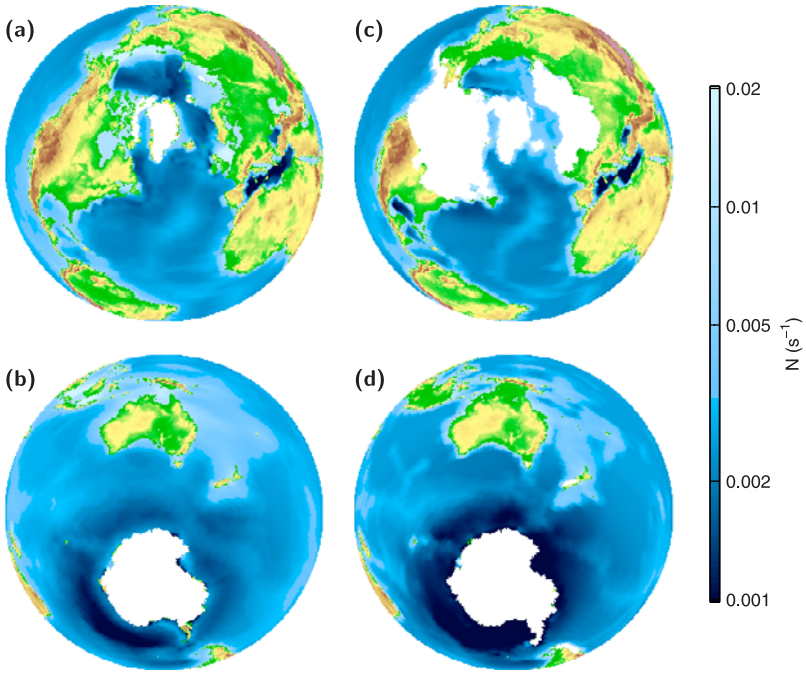

Figure 1. Continental location and ice location (from ICE-5G v 1.2, at 21 ka before present) and ocean stratification (from the climate simulations of *Peltier and Solheim* [2004]). Ice sheets are white, whilst the blue color scale gives the density stratification of the ocean (as vertically averaged buoyancy frequency N). (a) and (b) Present-day; (c) and (d) LGM.

to gravity, ζ_{EQ} is the equilibrium tide representing astronomical forcing, and ζ_{SAL} is the self-attraction and loading term [*Hendershott*, 1972], calculated using a spherical harmonic transform. The term $\mathbf{D}_{BL} = \rho c_d |\mathbf{u}|\mathbf{u}$, with $c_d = 0.0025$, parameterizes the drag of a turbulent bottom boundary layer. The term $\mathbf{D}_{IT}$ parameterizes internal tide drag. For a tide of frequency ω, we take

$$\mathbf{D}_{IT} = \frac{\rho N^2 H}{\omega}(\mathbf{u}\cdot\nabla H)\nabla H \times \begin{cases} 1 & |f| < \omega, \\ 0 & |f| > \omega, \end{cases}$$

where N is the vertically averaged buoyancy frequency. This original parameterization, which has similarities to that used by *Lyard et al.* [2006], is designed to account for internal wave generation by large steep topographic features, such as mid-ocean ridges, for which the internal tide is dominated by low order vertical baroclinic modes. The resulting deep-ocean dissipation for present-day semi-diurnal tides is about 40% of the total dissipation, consistent with observations [*Egbert and Ray*, 2003].

[7] The shallow-water equations are integrated forwards in time from rest, for a single tidal constituent. When equilibrium is reached, a tide is extracted using a harmonic analysis. We use a spherical coordinate system with the model pole running through 40°W and 75°N (Greenland) and its antipode (Antarctica). We make a Mercator transformation within this rotated system and then solve on a regular Arakawa C-grid, thus obtaining a solution with spatially varying resolution. For the results presented here (typically on a 720 × 720 grid), the grid spacing varies smoothly from about 55 km in the tropics to 5 km around the coast of Greenland and in the Ross Sea. The small grid spacing requires a time step of 30 s or less for numerical stability (we apply no spatial filtering), but the enhanced resolution at high latitudes is ideally suited for studying polar tides.

[8] In Figure 2, we present model results for the largest semi-diurnal constituent (M_2, of frequency 1.405×10^{-4} s^{-1}) and the largest diurnal constituent (K_1, of frequency 7.292×10^{-5} s^{-1}), which account for 68% and 11% of the tidal energy in the present-day ocean [*Egbert and Ray*, 2003]. Also shown are solutions for the present-day ocean, calculated using the corresponding topographic and stratification data sets. These are in excellent agreement with the data-constrained TPXO 6.2 global tidal solutions, an updated version of those described by *Egbert et al.* [1994], the average amplitude differences being 7 cm for M_2 and 2 cm for K_1. Here, the averages are calculated equatorward of 66° and in waters deeper than 1000 m, as is traditional [e.g., *Egbert et al.*, 2004]. The present-day M_2 solution is too energetic (with global energy 425 PJ), perhaps because of the sensitivity of this tide to the topography in the North Atlantic. The only deficiency in the present-day K_1 solution is a westward extension of the large tides in the Sea of Okhotsk.

[9] At LGM, the amplitude of the K_1 constituent remains relatively unchanged. Two exceptions are a considerable amplification in the South China Sea, previously noted by *Uehara* [2005], and an amplification around the coast of Antarctica. In contrast, the amplitude of the M_2 constituent changes considerably. There are several regions of small amplification (including around New Zealand, and the Caribbean), and two regions of considerable amplification.

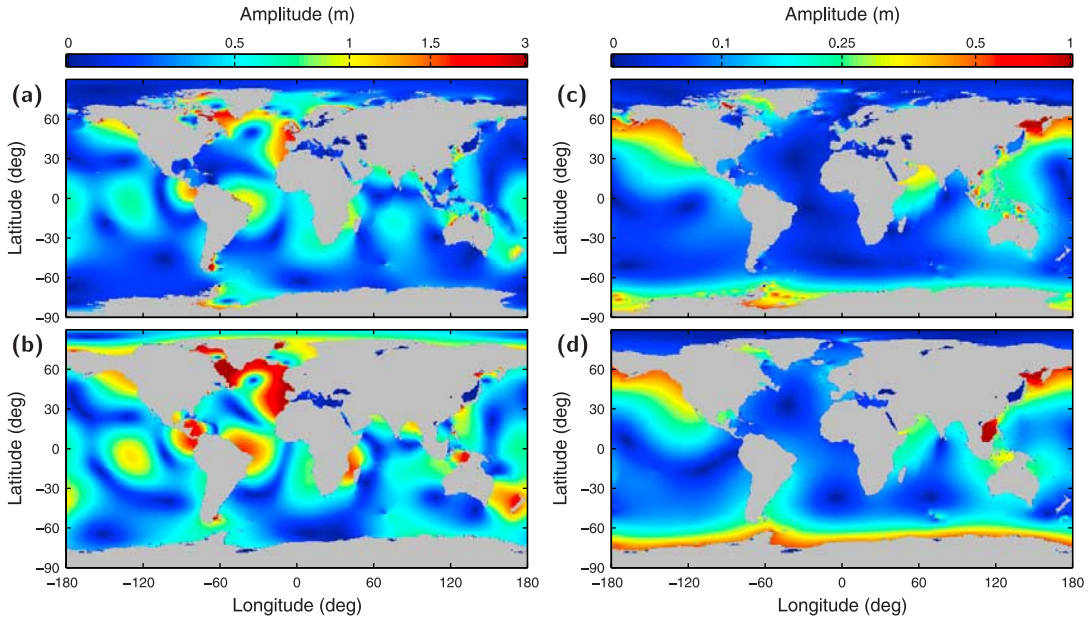

Figure 2. Modeled tidal amplitudes: (a) M_2, present-day; (b) M_2, LGM; (c) K_1, present-day; (d) K_1, LGM.

The first, in the North Atlantic, has been modeled previously [e.g., *Thomas and Sündermann*, 1999; *Egbert et al.*, 2004], and is associated with the blockage of the Hudson Strait by the Hudson Strait ice stream [*Arbic et al.*, 2004, 2007; *Uehara et al.*, 2006]. The second region of amplification is in the Arctic Ocean. This was not captured by recent high-resolution simulations [*Egbert et al.*, 2004; *Arbic et al.*, 2004] which excluded the Arctic Ocean for numerical purposes. All previous studies employed the ICE-4G data set for bathymetry [*Peltier*, 1994, 1996], and estimated stratification based on present-day values.

3. Arctic Tides

[10] A more detailed view of the M_2 Arctic tide is shown in Figure 3a (note the different color scale). The present day Arctic has only a small tide, but at LGM the tidal amplitude is 1–2 m along the entire coastline (Figure 3c), for this constituent alone. This amplification is entirely due to the change in the Arctic coastal configuration. With the closure of the Bering Strait, and the disappearance of the Barents Sea and the shallow waters surrounding the Queen Elizabeth Islands, the Arctic Ocean is almost entirely enclosed by land. Thus, Kelvin waves traveling around the coastline are trapped within the Arctic basin. Since the Kelvin wave speed $\approx\sqrt{gH}$ (for an ocean of uniform depth H, where g is the acceleration due to gravity), the Kelvin wave with zonal wavenumber n will have natural frequency ω_n given by

$$\omega_n \approx \frac{2\pi n\sqrt{gH}}{L}, \quad n = 1, 2, 3, \cdots \tag{1}$$

where L is the effective length of the Arctic coastline. Taking H = 3000 m and L = 7000 km (consistent with a coastline close to 80°N) implies $\omega_1 \approx 1.5 \times 10^{-4}$ s^{-1}. Thus, coastally confined zonal wavenumber one Kelvin waves are close to resonance at semi-diurnal frequencies.

[11] To test whether such Kelvin waves may explain the tides shown in Figure 3a, we calculate normal modes of the Arctic Ocean, which we isolate from the Atlantic by placing a wall at 80°N. For these calculations, we use a scalar approximation $\zeta_{SAL} = 0.08\zeta$ in the governing equations, and omit the drag terms $\mathbf{D}_{BL}$ and $\mathbf{D}_{IT}$. Using the same spatial resolution as for the time-dependent model (implying 20,000 grid points over the Arctic Ocean), we find a normal mode with frequency 1.403×10^{-4} s^{-1}, very close to the M_2 frequency. The amplitude of this mode (Figure 3b) has an almost identical structure to that of the modeled tide (Figure 3a). Snapshots of the surface displacement associated with this mode clearly reveal the character of a Kelvin wave with zonal wavenumber one. Kelvin waves with higher zonal wavenumbers appear at higher frequencies, consistent with equation (1).

[12] For the simulations presented, we modified the ICE-5G v 1.2 data set by placing grounded ice up to 79°N in the shallow seas around the present day Queen Elizabeth Islands (QEI), around 250°W. This approximately represents the farthest north that grounded ice is likely to have extended from the outflow of the Innuitian ice sheet [*England et al.*, 2006], which occupied the Canadian High Arctic and adjoined the much larger Laurentide and Greenland ice sheets. However, it is likely that the grounding line would have moved considerably during glacial periods [*Tarasov and Peltier*, 2004], and that during orbitally driven episodes of retreat the whole area around the QEI would have been occupied by a shallow sea, as in the ICE-5G v 1.2 data set. We have therefore performed additional simulations in this configuration. Over most of the globe, tidal amplitudes are unchanged. However, the M_2 tide is considerably amplified around the QEI (Figure 3d), reaching over 9 m in amplitude (Figure 3f). Repeating the normal-mode calculation in this configuration, the frequency of the zonal wavenumber one Kelvin mode falls to $1.332 \times$

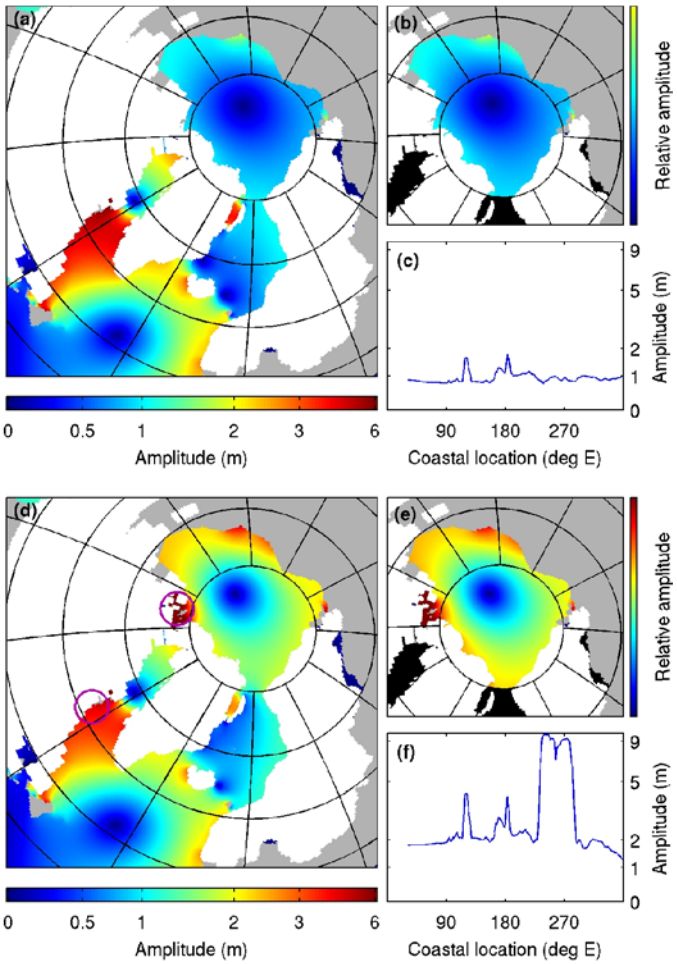

Figure 3. (a) Modeled LGM M_2 tidal amplitude. (b) Relative amplitude of the normal mode with frequency 1.403×10^{-4} s^{-1}. The oceans excluded from the normal-mode calculation are black. (c) Amplitude of the modeled M_2 tide along the Arctic coastline. The longitudes given are approximate, since the coastline winds back on itself in some places. (d) Modeled LGM M_2 tidal amplitude with the QEI surrounded by water. The purple circles show positions of two sources of ice-rafted debris. (e) Relative amplitude of the normal mode with frequency 1.332×10^{-4} s^{-1}. (f) Amplitude of the modeled M_2 tide along the Arctic coastline.

10^{-4} s^{-1}, and it too becomes rather localized around the QEI (Figure 3e).

[13] Although the pattern of the tides in the Arctic Ocean is determined locally, the direct astronomical forcing is weak and Arctic tides are excited by a northward flow of tidal energy from the Atlantic. For the cases of Figures 3a and 3d, the time-averaged northward energy fluxes through Fram Strait are 0.02 TW and 0.40 TW respectively. Thus, Arctic tidal amplitudes are greater in the second case, even though the Arctic normal mode is farther from resonance. We speculate that a greater energy flux is possible in this configuration because of the shallow seas around the QEI, where tidal dissipation is high. In this case, the energy flux of 0.40 TW is almost entirely balanced by a frictional dissipation via bottom drag of 0.37 TW, with all other terms (astronomical forcing, self-attraction and loading, and internal tide drag) negligible. This frictional dissipation accounts for 30% of the 1.2 TW of global dissipation via bottom drag, and 10% of the 3.6 TW of total global dissipation for M_2, which also includes 2.4 TW of internal tide dissipation. Thus, global dissipation increases markedly from the present day value of 2.44 TW, consistent with previous studies [*Egbert et al.*, 2004; *Uehara et al.*, 2006].

4. Tidal Interactions With Ice Streams

[14] It is therefore clear that large semi-diurnal tides along the entire Arctic coastline are inevitable during glacial periods, because of the robust Kelvin wave resonance equation (1), and that megatides are possible locally. Since during these periods the Arctic Ocean was partially surrounded by ice sheets, the tides would have interacted with ice streams and with any floating ice shelves connected to them, much as they do in present-day Antarctica [e.g., *Bindschadler et al.*, 2003; *Gudmundsson*, 2006]. Such interactions may have contributed in an important way to the instability of Arctic ice streams and ice shelves during the glacial period. For instance, large amplitude paleotides

might have led to heavily fractured ice shelves, either by tidal flexing of the shelf, or by the enhanced formation of crevasses near to the grounding line. Crevasses might have directly caused the break-up of ice shelves over time, or played a role in other destabilization mechanisms [e.g., *Hulbe et al.*, 2004].

[15] It has been speculated that modeled large semi-diurnal tides of the glacial Labrador Sea (also present in our ICE-5G based analyses) might have played a catalytic role in rapid destabilization of the Laurentide ice sheet at its primary discharge point near the present day Hudson Strait [*Arbic et al.*, 2004]. This was occupied by the Hudson Strait ice stream, whose instability is thought to have been the cause of quasi-periodic intense iceberg calving events that were characteristic of oxygen isotope stage 3 and are now referred to as Heinrich events [*Hemming*, 2004]. However, similar large rapid ice discharges originated from the Innuitian ice stream, close to the QEI [*Darby et al.*, 2002]. Since the largest Northern Hemisphere tides occur at just these two locations (see Figure 3d), the case is strengthened that tidal destabilization may have exerted a controlling influence upon these discharge events.

[16] Given the sensitivity of ice stream stability to conditions (including sea-level) near the grounding line [e.g., *Schoof*, 2007], it is possible that tides trigger, rather than merely catalyse, the destabilization of ice streams. For instance, when an ice stream is large enough to significantly alter the geometry of the coastline, and hence tidal amplitudes, destabilization could occur when the ice stream reached a certain extent. Such destabilization would be most likely to occur during a period of ice sheet growth, and would thus correlate with cold climate events. This is consistent with the timing of Heinrich events, which are apparently entrained to cold phases of the Dansgaard-Oeschger oscillation [e.g., *Sakai and Peltier*, 1998; *Hemming*, 2004]. It is clear that tides around the QEI would have been influenced by the extent of the Innuitian ice stream (compare Figures 3a and 3d), and it is likely that tidal amplitudes in a partially-open Hudson strait were similarly sensitive to the position of the Hudson strait ice stream. Mechanistic models of the linkage between tidal amplitude and the stability of ice streams under glacial conditions will be required to explore the detailed physics of this interconnection.

[17] **Acknowledgments.** Thanks to Guido Vettoretti for preparing the CSM 1.4 data set for our use and to Brian Arbic and Katsuto Uehara for preliminary discussions.

References

Adkins, J. F., K. McIntyre, and D. P. Schrag (2002), The salinity, temperature, and $\delta^{18}O$ of the glacial deep ocean, *Science*, *298*, 1769–1773.

Arbic, B. K., D. R. MacAyeal, J. X. Mitrovica, and G. A. Milne (2004), Palaeoclimate: Ocean tides and Heinrich events, *Nature*, *432*, 460, doi:10.1038/432460a.

Arbic, B. K., P. St-Laurent, G. Sutherland, and C. Garrett (2007), On the resonance and influence of the tides in Ungava Bay and Hudson Strait, *Geophys. Res. Lett.*, *34*, L17606, doi:10.1029/2007GL030845.

Bindschadler, R. A., M. A. King, R. B. Alley, S. Anandakrishnan, and L. Padman (2003), Tidally controlled stick-slip discharge of a west Antarctic ice stream, *Science*, *301*, 1087–1089.

Biton, E., H. Gildor, and W. R. Peltier (2008), Red Sea during the Last Glacial Maximum: implications for sea level reconstruction, *Paleoceanography*, *23*, PA1214, doi:10.1029/2007PA001431.

Darby, D. A., J. F. Bischof, R. F. Spielhagen, S. A. Marshall, and S. W. Herman (2002), Arctic ice export events and their potential impact on global climate during the late Pleistocene, *Paleoceanography*, *17*(2), 1025, doi:10.1029/2001PA000639.

Egbert, G. D., and R. D. Ray (2003), Semi-diurnal and diurnal tidal dissipation from TOPEX/Poseidon altimetry, *Geophys. Res. Lett.*, *30*(17), 1907, doi:10.1029/2003GL017676.

Egbert, G. D., A. F. Bennett, and M. G. G. Foreman (1994), TOPEX/POSEIDON tides estimated using a global inverse model, *J. Geophys. Res.*, *99*, 24,821–24,852.

Egbert, G. D., R. D. Ray, and B. G. Bills (2004), Numerical modeling of the global semidiurnal tide in the present day and in the Last Glacial Maximum, *J. Geophys. Res.*, *109*, C03003, doi:10.1029/2003JC001973.

England, J., N. Atkinson, J. Bednarski, A. S. Dyke, D. A. Hodgson, and C. Ó. Cofaigh (2006), The Innuitian Ice Sheet: Configuration, dynamics and chronology, *Quat. Sci. Rev.*, *25*, 689–703.

Garrett, C., and E. Kunze (2007), Internal tide generation in the deep ocean, *Annu. Rev. Fluid Mech.*, *39*, 57–87.

Gudmundsson, G. H. (2006), Fortnightly variations in the flow velocity of Rutford Ice Stream, West Antarctica, *Nature*, *444*, 1063–1064.

Hemming, S. R. (2004), Heinrich events: Massive late Pleistocene detritus layers of the North Atlantic and their global climate imprint, *Rev. Geophys.*, *42*, RG1005, doi:10.1029/2003RG000128.

Hendershott, M. C. (1972), The effects of solid earth deformation on global ocean tides, *Geophys. J. R. Astron. Soc.*, *29*, 389–402.

Hulbe, C. L., D. R. MacAyeal, G. H. Denton, J. Kleman, and T. V. Lowell (2004), Catastrophic ice shelf breakup as the source of Heinrich event icebergs, *Paleoceanography*, *19*, PA1004, doi:10.1029/2003PA000890.

Lyard, F., F. Lefevre, T. Letellier, and O. Francis (2006), Modelling the global ocean tides: Modern insights from FES2004, *Ocean Dyn.*, *56*, 394–415.

Peltier, W. R. (1994), Ice-age paleotopography, *Science*, *265*, 195–201.

Peltier, W. R. (1996), Mantle viscosity and Ice-Age ice sheet topography, *Science*, *273*, 1359–1364.

Peltier, W. R. (2004), Global glacial isostasy and the surface of the Ice-Age Earth: The ICE-5G (VM2) Model and GRACE, *Annu. Rev. Earth Planet. Sci.*, *32*, 111–149.

Peltier, W. R., and R. G. Fairbanks (2006), Global glacial ice volume and Last Glacial Maximum duration from an extended Barbados sea level record, *Quat. Sci. Rev.*, *25*, 3322–3337.

Peltier, W. R., and L. P. Solheim (2004), The climate of the Earth at Last Glacial Maximum: Statistical equilibrium state and a mode of internal variability, *Quat. Sci. Rev.*, *23*, 335–357.

Sakai, K., and W. R. Peltier (1998), Deglaciation-induced climate variability: An explicit model of the glacial-interglacial transition that simulates both the Bolling/Allerod and Younger-Dryas events, *J. Meteorol. Soc. Jpn.*, *76*, 1029–1044.

Schoof, C. (2007), Ice sheet grounding line dynamics: Steady states, stability, and hysteresis, *J. Geophys. Res.*, *112*, F03S28, doi:10.1029/2006JF000664.

Tarasov, L., and W. R. Peltier (2004), A geophysically constrained large ensemble analysis of the deglacial history of the North American ice-sheet complex, *Quat. Sci. Rev.*, *23*, 359–388.

Thomas, M., and J. Sündermann (1999), Tides and tidal torques of the world ocean since the Last Glacial Maximum, *J. Geophys. Res.*, *104*, 3159–3183.

Uehara, K. (2005), Changes of ocean tides along Asian coasts caused by the post glacial sea-level change, in *Mega-deltas of Asia: Geological Evolution and Human Impact*, edited by Z. Chen, Y. Saito, and S. L. Goodbred Jr., pp. 227–232, China Ocean Press, Beijing.

Uehara, K., J. D. Scourse, K. J. Horsburgh, K. Lambeck, and A. P. Purcell (2006), Tidal evolution of the northwest European shelf seas from the Last Glacial Maximum to the present, *J. Geophys. Res.*, *111*, C09025, doi:10.1029/2006JC003531.

Wunsch, C. (2005), Speculations on a schematic theory of the Younger Dryas, *J. Mar. Res.*, *63*, 315–333.

S. D. Griffiths and W. R. Peltier, Department of Physics, University of Toronto, 60 St. George Street, Toronto, ON, M5S 1A7 Canada. (sdg@atmosp.physics.utoronto.ca)